Cosmic-ray neutrinos in the atmosphere

T. K. Gaisser and Todor Stanev
Bartol Research Institute, University of Delaware, Newark, Delaware 19716

Giles Barr*
Department of Nuclear Physics, Oxford University, Keble Road, Oxford OX1 3NP, England
(Received 1 February 1988)

In this paper we give a complete account of detailed calculations of the flux of neutrinos of atmospheric origin that we have made for detectors at various locations on the globe. The emphasis here is on neutrinos in the energy range around 1 GeV, and we compare the results with recent measurements made with larger underground detectors. A detailed knowledge of the atmospheric cosmic-ray neutrino flux is a prerequisite for evaluating the background for the search for nucleon decay as well as the background for neutrinos of extraterrestrial origin.

I. INTRODUCTION

All large underground detectors, including the nucleon-decay detectors, record a significant number of neutrinos that interact within their fiducial volumes so that the interactions can be measured. These experiments are therefore also neutrino experiments for which the neutrino beam has to be calculated from the incident beam of cosmic-ray nucleons. The neutrino flux is different for each direction at each location as a consequence of the geomagnetic field, which cuts off the low-energy primary-cosmic-ray beam differently for each trajectory. Similarly, the neutrino flux varies in time because solar activity modulates the primary cosmic rays differently at different epochs, as the solar wind waxes and wanes.

We have calculated the fluxes of neutrinos in detail, taking into account these variations in the beam of primary nucleons and also accounting for details of production such as cascading in the atmosphere, energy losses of charged particles, and all relevant decay channels of pions, kaons, and hyperons. An outline of the calculation and some specific results have been published previously.[1,2] In this paper we describe the calculation fully and present the fluxes in a form that can be used by others as input to calculations of neutrino interaction rates in detectors at various locations. Numerical tables are available on request.

Neutrino interactions in underground detectors deserve attention for several reasons. First, they constitute the most important source of background for the search for nucleon decay, giving of order 3×10^{31} interactions per nucleon per year. In addition, neutrino detection can be used for intercalibration of detectors at different sites, and the angular dependence of the neutrino flux can put new limits on neutrino oscillation parameters. Finally, a good understanding of the atmospheric background is a perequisite for neutrino astronomy.

The calculation itself is also of interest. It can be adapted to calculate the neutrino beam from an astrophysical source given the spectrum of the accelerated primary beam and the distribution of target material at the source.[3]

The plan of the paper is as follows. In Section II we describe the calculation of the atmospheric neutrino beam. This has three components: the primary-cosmic-ray beam at the top of the atmosphere, the hadron interactions, and the simulation procedure itself. In Sec. III we present the calculated fluxes of electron-type and muon-type neutrinos: the vertical spectrum, the angular distributions at various locations, and the neutrino/antineutrino ratios. We also compare our results with those of previous calculations. Finally, in Sec. IV we discuss the comparison of the calculations with measurements of interaction rates of neutrinos at various detectors. Good agreement has been reported in several cases[4–7] in which the neutrino fluxes we have calculated for each site have been used by the experimental groups with their detector simulations to compute event rates and spectra of visible energy in the detectors.[8] It therefore appears that the atmospheric neutrino flux is well understood, though there is at present little information on ratios such as ν_e/ν_μ and neutrino to antineutrino. The remaining uncertainty in the background for nucleon decay therefore apparently has to do with the appearance of the neutrino interactions in each detector rather than with the neutrino flux itself.

II. CALCULATION OF ATMOSPHERIC NEUTRINO BEAM

Atmospheric neutrinos are produced when primary cosmic rays hit the atmosphere and initiate atmospheric cascades. Secondary mesons decay and give rise to neutrinos. The two essential components of the calculation are the energy dependence of the primary-cosmic-ray beam at the top of the atmosphere and the details of particle production in the atmosphere. Both must be known over several orders of magnitude in energy.

A. Primary nucleon beam

Nucleons with energy above the production threshold for pions arrive in the vicinity of the solar system with a

high degree of isotropy and approximately a power-law energy spectrum. They consist of free protons and of nucleons bound in nuclei (mostly helium). Because of interactions with the solar wind the lowest-energy particles cannot penetrate inside the heliosphere, so the primary spectrum in the vicinity of Earth has a maximum in the GeV region. The exact position of the maximum and the strength of the cutoff depends on the strength of the solar activity, which follows an eleven-year cycle.[9]

The intensity of the primary nucleon flux in the GeV region has been monitored by satellites,[10] and several balloon measurements of the absolute magnitude of the primary spectrum[11] have been performed at different stages of solar activity. These measurements, however, do not cover the entire energy region of interest, and errors in the magnitude of the flux appear to be quite high. At some energies, different experiments in a few cases differ by nearly a factor of 2. In general, different experiments are consistent to within about 30% in normalization. In order to quantify the uncertainty in the calculated neutrino flux due to uncertainties in the primary spectrum, we[12] carried out a review of the literature on the primary-cosmic-ray spectrum and composition. Table I shows the resulting "best fit" energy spectrum of primary nucleons that we finally adopted for this calculation.

To find the uncertainty in the neutrino flux we performed the calculation for an extreme "high" flux and an extreme "low" flux. These were obtained essentially by constructing[12] smooth envelopes of the data summary of Simpson.[11] In this way we estimate that there is an overall uncertainty of $\pm 10\%$ in calculated neutrino fluxes for $0.2 < E < 5$ GeV due to uncertainty in the normalization of the primary spectrum alone. This arises primarily from uncertainties in the 10–100 GeV range of primary energies, and is therefore not related to solar modulation.

Before the cosmic rays reach the atmosphere where they can interact and produce secondaries, they must also penetrate the geomagnetic field. Near the geomagnetic poles almost all primary particles can reach the atmosphere, moving along geomagnetic field lines. Close to the geomagnetic equator the field restricts the flux at the top of the atmosphere to particles with energies greater than a few tens of GeV, the exact value depending on the direction of the particle trajectory. Particles with magnetic rigidities below the local cutoff are bent away from Earth before they reach the atmosphere. Thus the energy spectrum of the primary beam is different for each direction at each location at each epoch of the solar cycle. We have used Cooke's calculations[13] of geomagnetic cutoffs to calculate the primary spectrum for each direction at each location. We have chosen to average the cutoffs over azimuth for each band of $\cos\theta$, where θ is the zenith angle. For a particular primary energy per nucleon E_0, the cutoff is represented by a number f_c $(0 < f_c < 1)$ which is the fraction of the region between two coaxial cones of half-angle $\theta_1 < \theta < \theta_2$ that is accessible to cosmic rays of that energy. The difference in cutoff energy per nucleon between protons and heavy nuclei was accounted for.

The cutoffs used here are those calculated for an offset dipole field. According to Cooke[13] the true cutoffs can differ by as much as 40% in particular directions. Moreover, there is a systematic underestimate of the cutoff near the horizon which would lead to an overestimate of the calculated neutrino flux. Considering also the uncertainties in the primary spectrum and the uncertainties in the hadronic interactions (see below), the overall uncertainty in the calculated neutrino fluxes is thus at least of order $\pm 20\%$. The comparison with contained events gives the needed confirmation of the normalization of the calculation.

TABLE I. Flux of primary nucleons ($m^{-2}s^{-1}sr^{-1}GeV^{-1}$).

Total E	Flux		Neutron fraction	
(GeV/nucleon)	$\odot_{min}$	$\odot_{max}$	$\odot_{min}$	$\odot_{max}$
2.0	1340	372	0.20	0.32
3.17	480	220	0.17	0.20
5.02	177	100	0.14	0.19
7.96	58	43	0.13	0.18
12.6	17	17	0.13	0.13
20	5.1	5.1	0.13	0.13
32	1.5	1.5	0.13	0.13
50	0.45	0.45	0.13	0.13
79.6	0.13	0.13	0.13	0.13
126	0.039	0.039	0.13	0.13
200	0.011	0.011	0.12	0.12
317	0.0033	0.0033	0.12	0.12
502	0.001	0.001	0.12	0.12

B. Hadron interaction model

Hadron interactions with energies from 1 to several hundred GeV contribute significantly to production of the atmospheric neutrinos responsible for contained events. Although hadron interactions with these energies have been studied in many accelerator experiments, not all relevant details of particle production on nuclear targets are well known. Typical spectrometer experiments have a milliradian solid angle of acceptance at a few settings of angle relative to the beam direction. Significant extrapolation and interpolation are needed to derive the inclusive cross sections integrated over transverse momentum, which we require for this calculation. The phase space is fully covered only in bubble chamber and emulsion experiments, which are not tailored for inclusive measurements.

As a framework for fitting data on hadronic interactions in airlike nuclei, we have used the parametrization of Stenlund and Otterlund,[14] which stems from systematic studies of hadronic interactions in nuclear emulsion over a large energy range. It distinguishes three interaction regions: projectile fragmentation, central, and target fragmentation. Particle production in these regions is described in terms of normalized pseudorapidity, and no distinction between the types of produced particles was made in the original parametrization. We have normalized the parametrization to proton interactions in light nuclei at a beam momentum of 24 GeV/c (Ref. 15). Details of charge ratio, K/pion ratio, and transverse-momentum distributions all as a function of longitudinal

momentum, were taken primarily from this experiment. We note that 24 GeV is roughly the median primary energy for cosmic-ray nucleons that gives rise to neutrinos above several hundred MeV. For orientation, we show in Fig. 1 some examples of response curves for neutrinos of various energies. The curves show the fraction of secondaries that are produced by primary nucleons with energies less than E.

The resulting interaction algorithm was extensively tested and its output compared to results of counter experiments on light, airlike targets.[16] In addition the model was tested and adjusted also to reproduce data at both ends of the energy interval of concern here, the TeV region and the region around several GeV. Its main features include leading-hadron elasticity skewed toward small values, energy-dependent cross sections rising from threshold, reaching plateaus of 265, 202, and 185 mb, respectively, for proton, pion, and kaon interactions in air around 3 GeV and then increasing as $\ln^{1.8}(s)$ above 100 GeV, charge conservation in individual interactions, and K/pion ratio increasing with energy to a value of 0.18 at 100 GeV and above.

The interaction algorithm does not use multiplicity as an input. Rather, particles are chosen from appropriate inclusive momentum distributions until all energy is used. Thus the multiplicity distribution and the energy dependence of the multiplicity become important tests of the performance of the model. Figure 2 shows a comparison between the average charged multiplicity from the program and the data of Ref. 16. Simulated multiplicity distributions are consistent with the accelerator data. The difference between the p-nucleus multiplicities and those for pp collisions,[17] also shown in Fig. 2, indicates the importance of using data from collisions on nuclei as the basis of a detailed calculation of fluxes produced in the atmosphere.

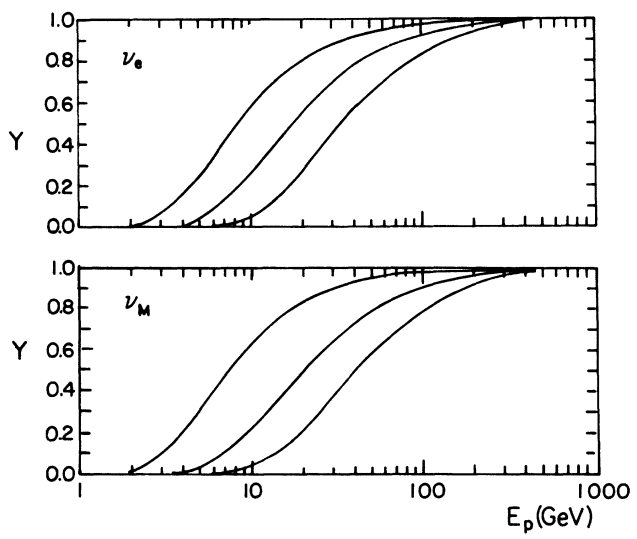

FIG. 1. Response curves for ν_μ and ν_e. The quantity plotted is the fraction of neutrinos that comes from primary nucleons with energies below E_p. Upper curves are for neutrinos with energy 0.3–0.4 GeV, middle ones for 1.0–1.1 GeV, and lower ones for 2–3 GeV.

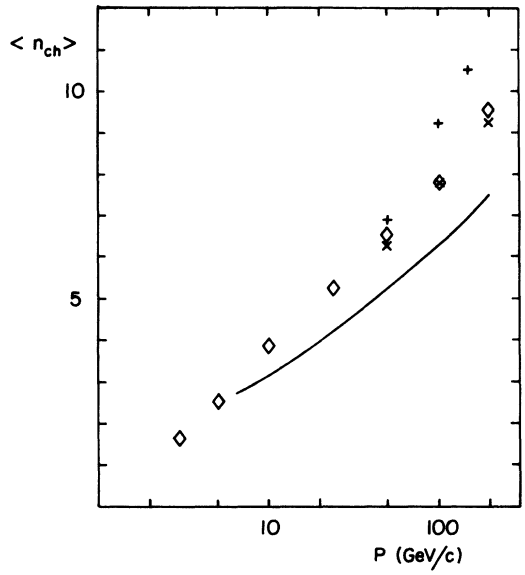

FIG. 2. Comparison of average charged multiplicity from the parametrization used in this calculation (diamonds) with various data. The solid line is the parametrization of measured multiplicities in pp collisions from Ref. 17. Crosses are from Braune *et al.* (Ref. 16) and ×'s from Barton *et al.* (Ref. 16). Both experiments in Ref. 16 are for protons on carbon.

C. Simulation procedure

The calculation of the neutrino beam consists of a number of Monte Carlo runs at many different discrete primary energies. The application of the Monte Carlo technique is important because of the lack of scaling, especially below 100 GeV, and the complications related to competition between interaction and decay and to energy loss in the atmosphere. In addition, the primary spectrum is not a simple power law at low energy, and, because of the geomagnetic cutoff, it is different for each location and direction. The calculation takes into account all secondary interactions in the atmosphere as well as the details of decay kinematics and of energy loss by charged particles. All decay branches with probability $> 1\%$ are included. To account for the relation between energy loss and decay probability the lifetimes are sampled in the particle rest system and the decay lengths are adjusted according to the actual energy loss in the atmosphere. The atmospheric model used is a fit by Shibata of the U.S. Standard Atmosphere.[18] For calculations of the yields in inclined cascades the relation between slant depth s and vertical depth in the atmosphere s_v was taken to be $s = s_v \sec\theta$ for angles up to 60°. At larger angles, where the curvature of Earth becomes important, the depth-height relation was tabulated and fitted for use in the program.

For each run at each nucleon energy and for each direction a table containing the yields of all four types of neutrinos classified by E_ν was constructed. Examples of the yields for certain neutrino energies and types are shown in Fig. 3. The neutrino yields were then folded with the primary nucleon spectrum, taking into account solar modulation and geomagnetic cutoffs for each direc-

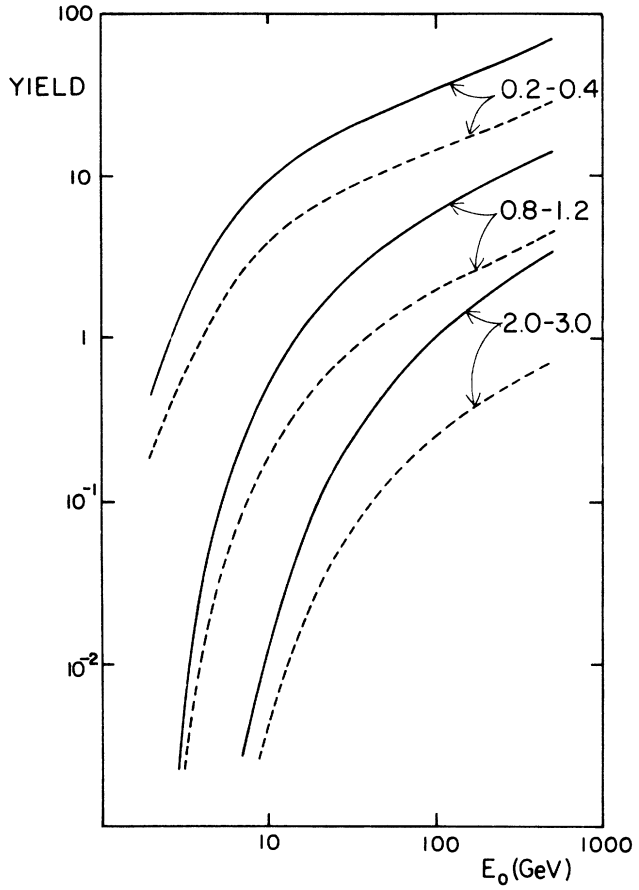

FIG. 3. Yields of neutrinos per incident proton as a function of proton energy. Solid lines for $\nu_\mu+\bar{\nu}_\mu$, dashed lines for $\nu_e+\bar{\nu}_e$ for three bins of neutrino energy, 0.2–0.4, 0.8–1.2, and 2–3 GeV. Yields are per GeV of neutrino energy.

tion. We also took account of the proton/neutron ratio, as indicated in the last two columns of Table I, in order to calculate correctly the $\nu/\bar{\nu}$ ratio and the muon charge ratio. Bound nucleons were treated in the superposition approximation, i.e., an incident nucleus of mass A and total energy E was treated as A-independent nucleons each of energy E/A. Finally, the spectrum-weighted yields were integrated to obtain the neutrino energy spectra for various directional bins at each location. The muon yields and energy spectra were obtained by the same procedure. This procedure is economical in the sense that the most time-consuming part of the calculation, Monte Carlo simulation of the yields, is done only once for each zenith angle. Applying the precalculated cutoffs, we then calculate the neutrino fluxes for different detector locations and solar epochs from the same yields.

The major remaining approximation in the calculation is that it is linear. For neutrinos from decay of stopped mesons this overestimates the flux by a factor of 2 since in reality half of these neutrinos go upwards. Even below 50 MeV, however, not all neutrinos are from stopped particles. Consequently, the overestimate of the flux in this "straight ahead" approximation is always less than a fac-

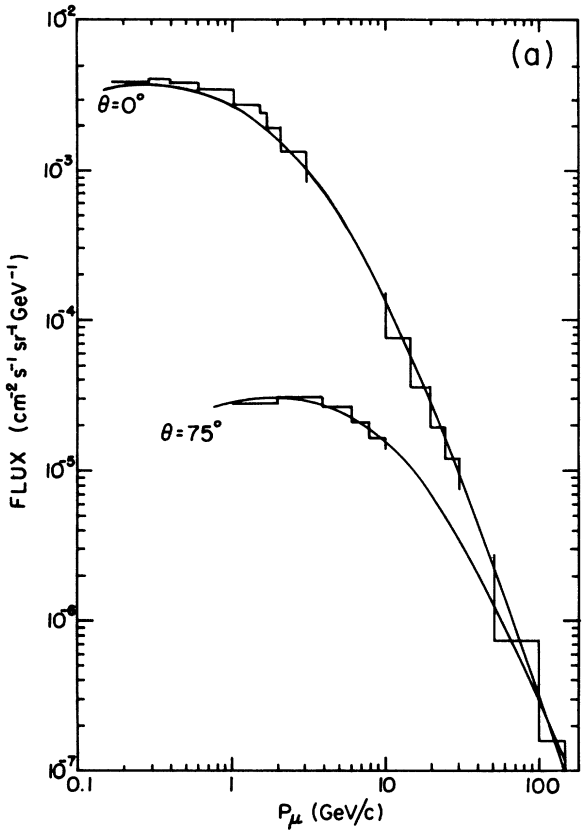

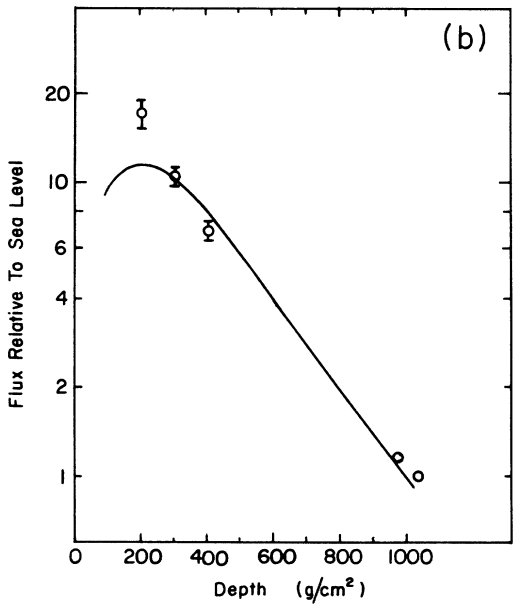

FIG. 4. Comparison of calculated muon fluxes with data. (a) Vertical and horizontal fluxes at sea level. Data of Refs. 20 (vertical) and 21 (horizontal) are represented by smooth curves; the calculations are given by histograms. (b) Vertical flux as a function of altitude. The data points are from Ref. 22.

TABLE II. Vertical fluxes of muons at sea level.

p_μ (GeV/c)	Data (Ref. 20)	Calculation
0.2	37	38
0.4	37	40
0.8	31	35
1.0	28	32
1.5	21	25
2.0	17	18
>3.0	37	36

tor of 2, and the estimate rapidly improves at higher energy. For neutrino energies greater than 200 MeV, the angle between the neutrino and its ancestral primary is usually less than 30°, and the linear calculation should reach its full accuracy. Lee and Bludman[19] have recently extended the calculation to three dimensions for certain directions of incidence. They find results within 20% of the linear calculation for E_ν between 50 and 200 MeV. The approximation is therefore completely adequate for calculation of the angular distribution of >200-MeV neutrinos, and it gives a useful estimate down to the lowest energies.

Comparison to measured fluxes of muons is a global test of the calculation. Figure 4(a) shows the comparison between calculation and data for spectra of vertical[20] and inclined[21] muons. A more detailed comparison in the low energy range is made in Table II. The low-energy fluxes at sea level are extremely sensitive to the details of muon energy loss. For example, the attenuation length deep in the atmosphere is roughly 370 g/cm^2 for muons in the momentum range 200–600 MeV/c. A 10% discrepancy in flux in this range thus corresponds to a path length difference of only 35 g/cm^2 out of a total vertical atmospheric thickness of 1033 g/cm^2. Some fraction of the difference between calculation and measurement in Table II may therefore be due to multiple scattering and detector resolution.

Because of the importance of energy loss, the relation between low-energy muons at sea level and low-energy neutrinos is complicated. Muons typically lose 2 GeV between production and decay, whereas the related neutrinos lose no energy. It is therefore of interest to calculate the muon flux as a function of altitude, though the corresponding measurements are limited.[22] Figure 4(b) shows the comparison. The agreement between experiment and calculation is again rather acceptable, with the exception of the highest altitude point. It is possible that the contribution of energetic pions to the measured flux at high altitude is significant,[23] contributing to the large measured value at the highest altitude. A more extensive comparison between the calculations and the muon fluxes and between this calculation and that of Ref. 23 is made elsewhere.[24]

III. NEUTRINO FLUXES

An early estimate of the flux of cosmic-ray-induced atmospheric neutrinos was made by Greisen,[25] and their use as a beam for studying neutrino interactions was suggested by Markov.[26] A first quantitative estimate of the spectrum of atmospheric neutrinos was made by Zatsepin and Kuz'min,[27] who included only the contribution from pions and muons. The contribution from kaons was included in the calculations of Refs. 28 and 29. The latter two calculations differ primarily in the way the muon flux is used to normalize the calculation. Cowsik, Pal, and Tandon[28] started from the primary nucleon flux and computed both neutrinos and muons. Osborne, Said, and Wolfendale[29] started with the measured muon flux and inferred the parent pion and kaon spectra, from which they then calculated the neutrino fluxes. In fact, at high energy, where muon decay and energy loss can be neglected, it is possible to write an approximate functional relation between the neutrino spectrum and the muon spectrum at sea level.[30]

The emphasis of the above calculations was on neutrino fluxes above 1 GeV, where details of muon energy loss and geomagnetic effects are of minor importance. Tam and Young,[31] calculated the neutrino spectrum down to 200 MeV using an expression[32] for the latitude and altitude dependence of the muon production spectrum, which was based on a series of measurements by Conversi[33] of the muon flux at various altitudes and latitudes. The calculation of Tam and Young therefore takes into account indirectly the geomagnetic cutoffs as well as the effects of muon energy loss.

The present calculation is conceptually simple. It starts from the primary spectrum and takes account of all these effects directly. A very detailed direct calculation of the neutrino spectrum at high energy is that of Volkova,[34] which uses a simple power-law primary spectrum and so cannot be extrapolated to below a few GeV. Together, however, the present calculation and that of Volkova give a quantitative, detailed representation of the spectra of atmospheric neutrinos from around 100 MeV to the highest energies. In the next subsection, we compare our results with those of Refs. 31 and 34 and with a recent calculation by Bugaev, Domogatsky, and Naumov.[35]

A. Vertical neutrino spectra

An unambiguous comparison with previous calculations can be made for the vertical flux of neutrinos at high geomagnetic latitude, where the cutoff plays no role. This is shown in Fig. 5. We find a flux of muon neutrinos uniformly higher than that of Tam and Young.[31] Our flux of electron neutrinos is somewhat higher below 1 GeV and about equal at high energy. In view of the totally different approach, it is impossible to identify the source of these differences. At the same time, we do not find such differences surprising, and we believe that the present more detailed direct calculation is more likely to be correct.

The differences between our spectra and those of Volkova[34] are easier to understand since both are direct calculations based on detailed treatment of the data on hadronic interactions. Volkova's calculation was aimed at higher-energy neutrinos, so she used a power-law primary spectrum proportional to $E_\nu^{-2.65}$ at all energies. This can account for the fact that her fluxes at 1 and 3 GeV are

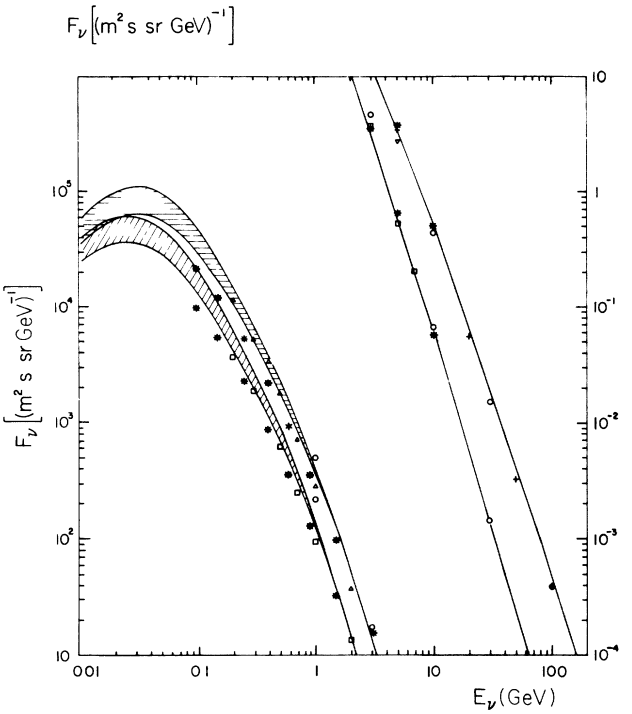

FIG. 5. Energy spectra of vertical neutrinos from various calculations. Our calculations are represented by the shaded bands in the low-energy region and by the smooth curves at high energies. The upper curve is the flux of $\nu_\mu+\bar{\nu}_\mu$ and the lower for $\nu_e+\bar{\nu}_e$. The top of each band is for solar minimum and the bottom for solar maximum. Other calculations are represented as follows: crosses, Ref. 29; triangles, Ref. 31(a); squares, Ref. 31(b); circles, Ref. 34; stars, Ref. 35.

higher than ours, because the primary spectrum that we use falls below the simple power law at low energy. Above 1000 GeV Volkova's fluxes are higher than ours because her primary spectrum is flatter. In the intermediate-energy range the somewhat higher value of the fluxes we calculate may be due in part to an increasing K/pion ratio and in part to the higher multiplicity of mesons in the model we use based on data taken with nuclear targets.

Comparison with the flux of Bugaev, Domugatsky, and Naumov,[35] is very interesting because, though the fluxes are rather different, the neutrino ratios are almost identical. For example, the ratio $(\nu_e+\bar{\nu}_e)/(\nu_\mu+\bar{\nu}_\mu)$ is 0.41 at 300 MeV and 0.34 at 1 GeV in both calculations, while our fluxes are nearly a factor of 2 higher at the lower energy and 30% higher at 1 GeV. At still higher energies the fluxes converge. For comparison, at 1 GeV Ref. 29 gives 0.32 for the ratio of electron-type to muon-type neutrinos, but Volkova[34] gives 0.44 for the ratio at 1 GeV. The high value of this ratio obtained by Volkova is not understood, though we note that she has used a rather high value of 16% for the K/π ratio and that 1 GeV is the lowest energy for which she has done the calculation. (We emphasize that the neutrino ratios in this paragraph are for vertical fluxes only; the ratio averaged over all angles is somewhat larger—see Sec. III C.) The authors of Ref. 35 attribute the difference in magnitude of the neutrinos flux between our calculation and theirs to a presumed difference in the parametrization of pion production. We note, however, that they have neglected pion regeneration by pions, which, though a small effect, goes in the right direction. We believe a more likely source of the difference in flux below $E_\nu \approx 1$ GeV is simply the primary spectrum used. The difference between low-energy fluxes at different extremes of the solar cycle in our calculation, as shown in Fig. 5, illustrates the sensitivity of the calculation to the normalization of the primary spectrum.

The early calculations do not extend below 100 MeV. With the increasing sophistication of underground detectors an estimate of the atmospheric neutrino flux below 100 MeV is now important. As mentioned above, the "straight ahead" approximation we use leads to an overestimate below 100 MeV (Ref. 19) but by less than a factor of 2. Thus the low-energy portion of the spectrum in Fig. 5 gives a useful first estimate. In particular, the position of the maximum around 35 MeV is determined by the kinematics of meson decay and is certainly a characteristic feature of the atmospheric spectrum.

B. Energy spectra and angular distributions

To present the neutrino distributions in a compact form, we give in Table III the fluxes averaged over all directions at solar maximum for four locations: Northern U.S. [Irvine-Michigan-Brookhaven (IMB) and Soudan], Western Europe [nucleon-stability experiment (NUSEX) and Frejus], Kamioka, and Kolar gold fields (KGF). Figure 6 shows the ratio of fluxes at solar minimum to solar maximum, averaged over all angles. There are two interesting features of the solar modulation of the neutrino flux. First, the effect is larger at higher geomagnetic latitudes where the contribution from the low-energy part of the primary spectrum, which suffers the most modulation, is greatest. (Even though KGF is at a lower latitude than Kamioka the modulation can be similar because of the averaging over all directions of incidence.) Second, the modulation is greatest around 35

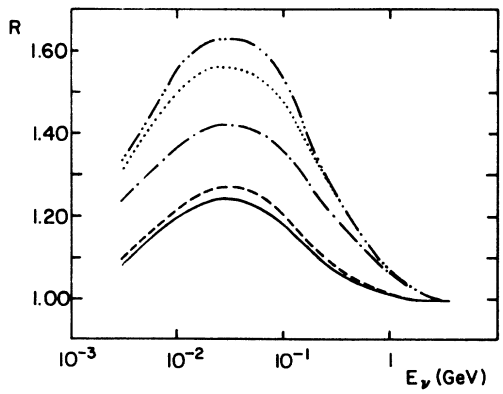

FIG. 6. Ratio of $\nu_\mu+\bar{\nu}_\mu$ fluxes at solar minimum to those at solar maximum for various locations. The curves from highest to lowest are for Soudan, IMB, Mont Blanc/Frejus, KGF, and Kamioka. The corresponding ratios for electron neutrinos are practically the same.

MeV where the neutrino spectrum peaks and is in fact smaller for very low neutrino energies. This is a reflection of kinematics: 30 MeV is the energy of the neutrino from decay at rest of a pion, and the mean energy of a neutrino from decay of a stopped muon is about 35 MeV. Lower-energy neutrinos must originate from decay in flight with the neutrino projected backward in the rest frame of the parent meson. The lower the neutrino energy (below ≈ 35 MeV) the more energetic the parent and the less the modulation.

In Fig. 7 we show the angular distributions relative to the average for energies from 200 MeV to 3 GeV, averaged over the solar cycle. In the energy range from 0.2 to 2 GeV the angular distribution of the neutrino flux has a dual origin. First, the relative probability of decay is larger for mesons in slanting showers than in vertical showers, which leads to the peak in the distribution near the horizontal. (As pointed out by Lee and Bludman,[19] however, this is somewhat suppressed in the more realistic three-dimensional calculation because projection of neutrinos out of the atmosphere is more likely for cascades near the horizontal.) The other factor is the geomagnetic field, which creates different cutoffs for each zenith angle at each location. Neutrinos with energy several GeV and higher are generated by primary nucleons of energy too high to be affected by the geomagnetic field, so the second factor is not relevant at high energy. On the other hand, the geometrical path through the atmosphere becomes short compared to the decay lengths (about 60 km for a 10-GeV muon). At these energies the competition between interaction and decay for pions begins to be important, so the neutrino flux is higher near the horizontal because the parent pions and kaons have a larger path length for decay in the tenuous upper atmosphere. The net result is that neutrino production roughly follows the overall thickness of the atmosphere. For angles to about 60° it is approximately proportional to secant of the zenith angle, and at larger angles the effect of the finite radius of Earth slows down the increase.

C. Neutrino ratios

The principal sources of neutrinos are decays of pions, kaons, and muons. The decay chain from pions is

$$\begin{aligned} \pi^{\pm} &\rightarrow \mu^{\pm} + \nu_{\mu}(\bar{\nu}_{\mu}) \\ &\quad \big\lfloor \rightarrow e^{\pm} + \nu_e(\bar{\nu}_e) + \bar{\nu}_{\mu}(\nu_{\mu}) \ , \end{aligned} \tag{1}$$

with a similar chain for charged kaons. In the low-energy limit where all particles decay we therefore expect

$$\nu_{\mu} + \bar{\nu}_{\mu} \approx 2(\nu_e + \bar{\nu}_e) \tag{2}$$

and

$$\nu_e / \bar{\nu}_e \approx \mu^+ / \mu^- \ . \tag{3}$$

Moreover, the kinematics of π and μ decay is such that roughly equal energy is carried on average by each neutrino in the chain.

TABLE III. Angular-averaged ν fluxes $(\mathrm{m^2 sr\ s\ bin})^{-1}$.

Site / E (GeV)	Northern U.S.				Kamiokande				Mt. Blanc/Frejus				KGF (India)			
	ν_e	$\bar{\nu}_e$	ν_{μ}	$\bar{\nu}_{\mu}$	ν_e	$\bar{\nu}_e$	ν_{μ}	$\bar{\nu}_{\mu}$	ν_e	$\bar{\nu}_e$	ν_{μ}	$\bar{\nu}_{\mu}$	ν_e	$\bar{\nu}_e$	ν_{μ}	$\bar{\nu}_{\mu}$
0.002–0.004	5.9	5.2	5.8	5.9	3.8	3.4	4	4	5.3	4.8	5.4	5.5	3.1	2.8	3.3	3.3
0.008–0.01	18	16	25	25	10	10	15	15	16	14	22	22	8.5	7.9	12	12
0.02–0.03	145	130	240	240	78	73	130	130	121	112	203	203	63	60	105	105
0.03–0.04	140	126	245	245	75	71	130	130	117	108	206	207	62	57	107	108
0.04–0.06	230	210	435	434	130	120	235	235	197	183	370	370	104	98	190	190
0.06–0.08	180	160	350	350	97	94	195	195	150	140	300	300	81	76	160	160
0.08–0.1	136	122	280	280	78	74	160	160	118	108	240	240	64	60	130	130
0.2–0.4	250	220	530	530	180	165	380	380	240	210	500	500	145	135	310	310
0.4–0.6	90	78	190	190	69	63	150	150	87	76	186	185	58	53	127	126
0.6–0.8	42	36	92	91	34	31	77	76	41	35	90	90	29	26	66	65
0.8–1.0	23	19	51	50	20	17	45	44	23	19	50	50	17	15	39	38
1.0–1.2	14	12	31	31	12	10.5	28	28	14	11	30	30	10.5	9.2	24	24
1.2–1.4	9.0	7.3	20	20	8.0	6.8	19	18	8.9	7.3	20	20	7.0	6.0	16.5	16
1.4–1.6	6.2	5.0	14	14	5.6	4.7	13	13	6.1	5.0	14	14	5.0	4.2	12	11
1.6–1.8	4.3	3.5	10	9.8	4.0	3.3	9.5	9.1	4.3	3.5	10	9.7	3.6	3.0	8.6	8.3
1.8–2.0	3.1	2.5	7.2	7.3	2.9	2.4	6.9	6.9	3.1	2.5	7.2	7.3	2.6	2.2	6.3	6.3
2.0–3.0	7.5	5.9	18	18	7.1	5.7	18	17	7.5	5.9	18	18	6.6	5.4	17	16
>3.0	5.4	4.2	16	15	5.3	4.1	16	15	5.4	4.2	16	15	5.1	4.0	15	14

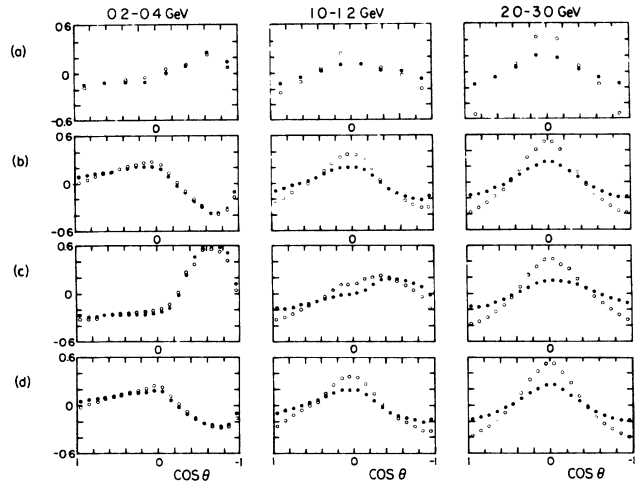

FIG. 7. Angular distributions of neutrinos relative to the average for four locations. The quantity plotted is $(F-\langle F\rangle)/\langle F\rangle$. Open circles represent $\nu_e+\bar{\nu}_e$ and solid circles represent $\nu_\mu+\bar{\nu}_\mu$. The four locations are, from top to bottom, Kamioka, IMB, KGF, Mont Blanc/Frejus. Upward-going neutrinos have $\cos\theta=-1$.

The ratio $(\nu_\mu+\bar{\nu}_\mu)/(\nu_e+\bar{\nu}_e)$ is shown in Fig. 8 averaged over angles and over the solar cycle. The vertical size of the boxes reflects the range of this ratio for various detectors, which is small. The horizontal size of the box simply reflects the binning. In the region around $E_\nu\approx 100$ MeV the ratio is about two, as expected when all mesons decay. At high energies the muon decay path $E_\mu c\tau/\mu$ becomes larger than the thickness of the atmosphere. (For vertical muons this occurs for $E_\mu \gtrsim 2$ GeV, and at somewhat higher energy for inclined muons.) In the high-energy limit muon decay no longer contributes and the main contribution to the flux of electron neutrinos is from decay of neutral kaons. At very low energies the ratio of neutrino flavors approaches 1. This again is a consequence of kinematics: the Michel spectrum for neutrinos from muon decay, when transformed into the laboratory, peaks at $E_\nu=0$ (Ref. 27). Thus the very-low-energy neutrinos come preferentially from muon decay, giving a ratio near one.

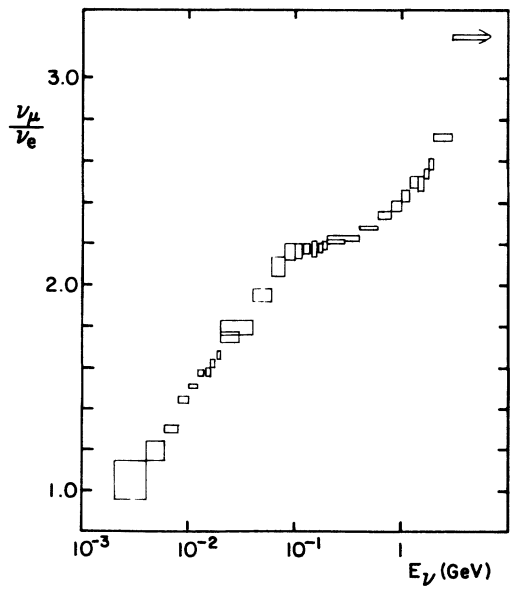

FIG. 8. The ratio $(\nu_\mu+\bar{\nu}_\mu)/(\nu_e+\bar{\nu}_e)$.

The ratio of neutrinos to antineutrinos is shown in Fig. 9. A neutrino excess of order of 20% derives ultimately from the preponderance of protons in the primary beam, together with charge conservation and the tendency of fast secondaries to reflect the charge of the interacting hadron. Electron and muon neutrinos show quite different behavior due to the decay characteristics of the parents. Since

$$\pi^+\rightarrow\nu_\mu+\mu^+ \quad \text{and} \quad \mu^+\rightarrow\bar{\nu}_\mu\ ,$$

one expects $\nu_\mu/\bar{\nu}_\mu=1$ at low enough energy for all muons to decay. Thus the ratio $\nu_\mu/\bar{\nu}_\mu$ depends on the fraction of muons that go through the atmosphere without decaying. As energy increases, fewer muons decay and the ratio $\nu_\mu/\bar{\nu}_\mu$ approaches the parent π^+/π^- ratio, first in the vertical direction and at higher energy in the horizontal direction. On the other hand, electron neutrinos of all energies reflect the charge asymmetry of the primaries. Indeed, the effect increases at high energy as a larger fraction of electron neutrinos originate from kaon decay.

D. Charge ratio of muons

We obtain the μ^+/μ^- ratio as a by-product of the neutrino calculation. In previous calculations there has

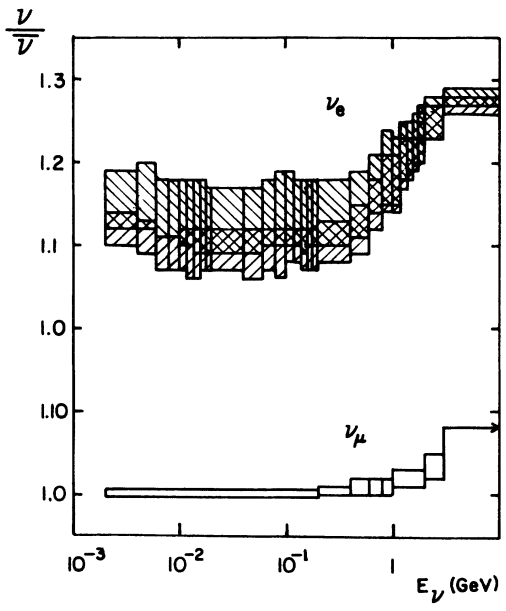

FIG. 9. Ratio of neutrinos to antineutrinos. For electron neutrinos the upper band is for solar minimum and the lower band is for solar maximum. The vertical size of each band reflects the differences among different locations. The top of each band is for Soudan and the bottom for Kamioka and KGF. IMB is just below the top and Mont Blanc/Frejus between. (See Table III.)

sometimes been a tendency to obtain higher values than measured. We find $\mu^+/\mu^- = 1.21 \pm 0.02$ for the momentum range 1–3 GeV/c. The corresponding measurements[36] are 1.18 ± 0.02 at 1 GeV/c increasing to 1.25 ± 0.02 in the range 2–3 GeV/c. The agreement here is a consequence of taking account of the ratio of neutrons to protons in the incident beam together with use of data from hadron collisions on nuclei as the basis of the cascade calculation. For calculations of the ratios we have assumed that neutrino production by protons is the same as antineutrino production by neutrons and vice versa. (This is strictly true for all neutrinos except those from kaons produced in association with leading strange baryons.[24])

IV. CONCLUSION: COMPARISON WITH OBSERVED NEUTRINO FLUXES

The rate of contained events induced by the neutrino flux is

$$R = N_A M_f \sum_i \int \left[\int \frac{d\sigma_i}{dE_{\rm vis}} \frac{dN_\nu^i}{dE_\nu} dE_\nu d\Omega \right] \epsilon_i(E_{\rm vis}) dE_{\rm vis} ,$$

where dN_ν^i/dE_i is the flux of neutrinos of the ith flavor, $d\sigma_i/dE_{\rm vis}$ is the cross section per nucleon for interaction of ν_i to produce visible energy $E_{\rm vis}$ in the detector, and ϵ_i is the experimental efficiency for containing and detecting a particular type of event with its vertex inside the fiducial volume. A complete quantitative comparison requires use of the Monte Carlo event generator for each detector to account correctly for the detection efficiency. The comparison made by the IMB group[4] between calculation and measurement is reproduced in Fig. 10.

Since most of the target nucleons in the nucleon decay experiments are bound in nuclei, it is necessary to use the appropriate cross sections for lepton production off bound nucleons. The difference from cross sections on free nucleons becomes important for lepton energies below 300–400 MeV (Ref. 37). Comparison with the quasielastic events from the Kamioka experiment (which extend to lower energy) is made in Ref. 37. Again the agreement is quite good.

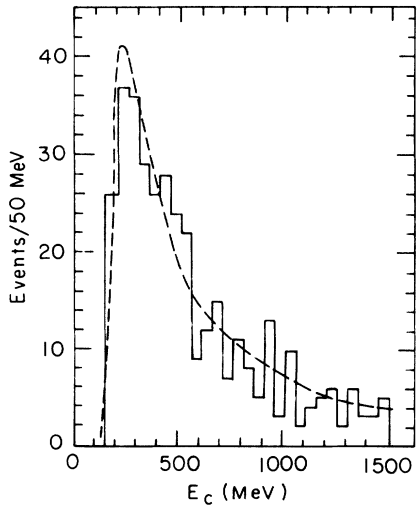

FIG. 10. Comparison between calculated and measured spectrum of contained neutrino interactions in IMB (from Ref. 4).

In Table IV we summarize the comparisons made by the various experimental groups[4–7,38] between expected events induced by atmospheric neutrinos and observed rates of contained events. The KGF group used the neutrino fluxes of Ref. 29 and the others used the neutrino fluxes from this calculation. These comparisons, as well as comparisons between expected and observed distributions of visible energy, are summarized by Ayres *et al.*[8] In all cases the agreement is excellent. It is therefore clear that the rates of contained events can be understood entirely in terms of interactions of atmospheric neutrinos. There is no evidence for an excess of events due to nucleon decay or to extraterrestrial sources of neutrinos. As emphasized in Refs. 4–7, identification of nucleon decay depends on identifying a subset of events whose appearance and rates in the detector are inconsistent with configurations typical of neutrino interactions. Conversely, assuming that most of the contained events are indeed due to interactions of atmospheric neutrinos, the measurements confirm the normalization and shape of the calculated neutrino spectra in the range from 100 MeV to 3 GeV to within the present statistics of order of 1000 events. We note, however, that discrimination between electron and muon neutrinos is difficult, especially in the water detectors. As a consequence, this aspect of the calculation has not yet been very well tested.

Fluxes of atmospheric neutrinos above a few GeV give rise to an external signal of upward muons induced by interactions of muon-type neutrinos in the material surrounding the detector. Here again, the calculated rates are in agreement with what is observed.[39]

To summarize, there is at present no evidence for an excess of extraterrestrial neutrinos above the atmospheric background, with two notable exceptions: solar neutrinos[40] and the neutrino burst from SN1987A (Refs. 41 and 42). For these neutrinos with energies of tens of MeV (and in the case of SN1987A a sharp time structure) the background induced by atmospheric neutrinos is orders of magnitude less than the signal.[43] Comparison between the atmospheric background and the signal of multi-GeV neutrinos expected if the Sun is concentrating dark-matter candidates, has been made by many authors.[44] Some candidates, such as sneutrinos, are ruled out by present measurements, and the sensitivity of present detectors is in a very interesting range for others, such as

TABLE IV. Numbers of neutrino interactions.

Detector	Exposure (kT yr)	Measured	Calculated
KGF	0.28	23	17
NUSEX	0.42	37	37
Frejus	0.6	65	60
IMB	3.8	401	403
Kamiokande	1.5	181	170

photinos and Higgsinos. Multi-TeV neutrinos from sources such as Cygnus X-3 may be well above the background induced by the steep atmospheric flux[45] but their signal is probably too low to be seen by present detectors.

Note added in proof. Effects due to muon polarization were not included in this calculation. We are grateful to L. Volkova for pointing out to us that this is likely the source of our lower value of the ν_e/ν_μ ratio for vertical muons at 1 GeV. The quantitative effect on the ratio averaged over angle and energy, and its relation to the recently reported measurement of the ratio by the Kamioka group, is currently under investigation.

ACKNOWLEDGMENTS

We are grateful to D. H. Perkins, J. C. van der Velde, and A. K. Mann for helpful discussions. We thank J. A. Simpson and M. Garcia-Munoz for supplying us with detailed references for compilation of the data on primary spectra. This work was supported in part by the U.S. Department of Energy under Contact No. DE-AC02-078ER05007 and by the National Science Foundation under Grant No. PHY-8613080. G.D.B. acknowledges support by the U.K. Science and Engineering Research Council.

---

*Present address: CERN, Geneva, Switzerland.

[1]T. K. Gaisser, Todor Stanev, S. A. Bludman, and H. Lee, Phys. Rev. Lett. **51**, 223 (1983); in *Proceedings of the Fourth Workshop on Grand Unification*, Philadelphia, Pennsylvania, 1983, edited by A. Weldon, P. Langacker, and P. J. Steinhardt (Birkhauser, Boston, 1983), p. 87.

[2]T. K. Gaisser and Todor Stanev, in *Proceedings of the 11th International Conference on Neutrino Physics and Astrophysics*, Dortmund, West Germany, 1984, edited by K. Kleinknecht and E. A. Paschos (World Scientific, Singapore, 1984), p. 370, and references therein. Also T. K. Gaisser and Todor Stanev, in *Proceedings of the Sixth Workshop on Grand Unification*, Minneapolis, Minnesota, 1985, edited by Serge Rudaz and Thomas F. Walsh (World Scientific, Singapore, 1986), p. 236.

[3]T. K. Gaisser and Todor Stanev, Phys. Rev. Lett. **54**, 2265 (1985), **58**, 1695 (1987); **59**, 844(E) (1987).

[4]T. J. Haines *et al.*, Phys. Rev. Lett. **57**, 1986 (1986); in *Proceedings of the Sixth Workshop on Grand Unification* (Ref. 2), p. 42, and references therein.

[5]Kamiokande Collaboration, M. Nakahata *et al.*, J. Phys. Soc. Jpn. (to be published).

[6]Frejus Collaboration, F. Raupach, in *New and Exotic Phenomena*, edited by O. Fackler and J. Tran Thanh Van (Editions Frontières, Gif-sur-Yvette, France, 1987), p. 35.

[7]NUSEX Collaboration, E. Belloti *et al.*, in *Massive Neutrinos in Particle Physics and Astrophysics*, proceedings of the Twenty-First Rencontre de Moriond (Sixth Workshop), Tignes, Savoie, France, 1986, edited by O. Fackler and J. Tran Thanh Van (Editions Frontières, Gif-sur-Yvette, France, 1986), p. 165.

[8]For recent reviews and references to the experiments, see D. S. Ayres *et al.*, in *Proceedings of the Summer Study on the Physics of the Superconducting Super Collider*, Snowmass, Colorado, 1986, edited by R. Donaldson and J. Marx (Division of Particles and Fields of the APS, New York, 1987); T. Stanev, Rapporteur paper, in *Proceedings of the Nineteenth International Cosmic Ray Conference*, La Jolla, California, 1985, edited by F. C. Jones, J. Adams, and G. M. Mason (NASA Conf. Publ. No. 2376) (Goddard Space Flight Center, Greenbelt, MD, 1985), Vol. 9, p. 383; J. C. van der Velde, in *First Aspen Winter Physics Conference*, Aspen, Colorado, 1985, edited by Martin M. Block (Ann. N. Y. Acad. Sci. Vol. 461) (New York Academy of Science, New York, 1985), p. 615; and D. H. Perkins, Annu. Rev. Nucl. Part. Sci. **34**, 1 (1984).

[9]M. A. Pomerantz and S. P. Duggal, Rev. Geophys. Space Phys. **12**, 343 (1974).

[10]M. Garcia-Munoz *et al.*, J. Geophys. Res. **91**, 2858 (1986).

[11]For compilations of data, see J. Ormes and P. Freier, Astrophys. J. **222**, 471 (1978); J. A. Simpson, Annu. Rev. Nucl. Part. Sci. **33**, 323 (1983).

[12]Giles Barr and T. K. Gaisser, Soudan 2 Internal Note PDK-281, Oxford, 1986 (unpublished).

[13]D. Cooke, Phys. Rev. Lett. **51**, 320 (1983), has published cutoffs for locations of major experiments. His results were obtained from the Stormer relation for a dipole field with its center offset from the center of Earth.

[14]E. Stenlund and I. Otterlund, CERN Report No. EP/82-42 (unpublished). See also I. Otterlund, Nucl. Phys. **A418**, 87c (1984), and references therein.

[15]T. Eichten *et al.*, Nucl. Phys. **B44**, 333 (1972). See, also, J. V. Allaby *et al.*, CERN Report No. EP/70-12 (unpublished).

[16]K. Braune *et al.*, Z. Phys. C **17**, 105 (1983); D. S. Barton *et al.*, Phys. Rev. D **27**, 2580 (1983).

[17]M. Antinucci *et al.*, Lett. Nuovo Cimento **6**, 121 (1973).

[18]S. E. Forsythe, *Smithsonian Physical Tables* (Smithsonian Institution Press, Washington, D.C., 1969). The fit of Shibata is described in T. K. Gaisser, M. Shibata, and J. A. Wrotniak, Bartol Report No. 81-21 (unpublished).

[19]H. Lee and S. A. Bludman, Phys. Rev. D **37**, 122 (1988).

[20]O. C. Allkofer, K. Carstensen, and W. D. Dau, Phys. Lett. **36B**, 425 (1971).

[21]A. Jokisch *et al.*, Phys. Rev. D **19**, 1368 (1979).

[22]M. Conversi, Phys. Rev. **79**, 749 (1950).

[23]D. H. Perkins. Oxford University Report No. 85/84 (unpublished).

[24]G. D. Barr and T. K. Gaisser, Soudan 2 Internal Note PDK-338, Oxford, 1987 (unpublished).

[25]K. Greisen Annu. Rev. Nucl. Sci. **10**, 63 (1960).

[26]M. A. Martov, in *Proceedings of the Tenth Annual International Conference on High Energy Physics*, Rochester, New York, 1960, edited by E. C. G. Sudarshan, J. H. Tinlot, and A. C. Mellissinos (Interscience, New York, 1960).

[27]G. T. Zatsepin and V. A. Kuz'min, Zh. Eksp. Teor. Fiz. **41**, 1818 (1961) [Sov. Phys. JETP **14**, 1294 (1962)].

[28]R. Cowsik, Yash Pal, and S. N. Tandon, Proc. Indian Acad. Sci. **63**, 217 (1966).

[29]J. L. Osborne, S. S. Said, and A. W. Wolfendale, Proc. Phys. Soc. London **86**, 93 (1985). See also J. L. Osborne, in *Cosmic Rays at Ground Level*, edited by A. W. Wolfendale (Hilger,

London, 1973), p. 85.
[30]M. Koshiba, Prog. Theor. Phys. **41**, 832 (1969). See also S. Hayakawa, *Cosmic Ray Physics* (Wiley-Interscience, New York, 1969), p. 404.
[31](a) A. C. Tam and E. C. M. Young, in *Proceedings of the Eleventh International Conference on Cosmic Rays,* Budapest, 1969, edited by P. Gombás [Acta Phys. Acad. Sci. Hung. Suppl. **4**, 307 (1970)]. (b) See E. C. M. Young, in *Cosmic Rays at Ground Level* (Ref. 29), p. 105.
[32]S. Olbert, Phys. Rev. **96**, 1400 (1954).
[33]Conversi (Ref. 22). The latitude dependence was measured by carrying the instrument on a B-29 at 30 000 feet from China Lake, California south to the equator and north to Alaska. The altitude dependence was measured at northern latitudes and corrected to 50° N.
[34]L. V. Volkova, Yad. Fiz. **31**, 1510 (1980) [Sov. J. Nucl. Phys. **31**, 784 (1980)].
[35]E. V. Bugaev, G. V. Domogatsky, and V. A. Naumov, in *Cosmic Ray Muon and Neutrino Physics/Astrophysics Using Deep Underground/Underwater Detectors,* proceedings of the Japan-U. S. Seminar, edited by Y. Ohashi and V. Z. Peterson (Institute for Cosmic Ray Research of the University of Tokyo, Tokyo, 1986).
[36]O. C. Allkofer and P. K. F. Grieder, Physics Data No. 25-1, 1984.
[37]T. K. Gaisser and J. S. O'Connell, Phys. Rev. D **34**, 822 (1986).
[38]M. R. Krishnaswamy *et al.,* Pramana **19**, 525 (1982).
[39]T. K. Gaisser and Todor Stanev, Phys. Rev. D **30**, 985 (1984). See also Gaisser and Stanev, in *Proceedings of the Sixth Workshop on Grand Unification* (Ref. 2).
[40]J. K. Rowley, B. T. Cleveland, and R. Davis, Jr., in *Solar Neutrinos and Neutrino Astronomy,* Lead, South Dakota, 1984, edited by M. L. Cherry, W. A. Fowler, and K. Lande (AIP Conf. Proc. No. 126) (AIP, New York, 1985), p. 1.
[41]K. Hirata *et al.,* Phys. Rev. Lett. **58**, 1490 (1987).
[42]R. M. Bionta *et al.,* Phys, Rev. Lett. **58**, 1494 (1987).
[43]T. K. Gaisser and Todor Stanev, in *Solar Neutrinos and Neutrino Astronomy* (Ref. 40), p. 277.
[44]See, for example, T. K. Gaisser, Gary Steigman, and S. Tilav, Phys. Rev. D **34**, 2206 (1986); K.-W. Ng, K. Olive, and M. Srednicki, Phys. Lett. B **188**, 138 (1987); J. Ellis, R. A. Flores, and S. Ritz, *ibid.* **198**, 393 (1987); S. Ritz and D. Seckel, Report No. CERN-TH. 4627, 1987 (unpublished); Keith A. Olive and Mark Srednicki, Report No. UMN-TH-636/87 (unpublished).
[45]Gaisser and Stanev, in *Proceedings of the Nineteenth International Cosmic Ray Conference* (Ref. 2), Vol. 8, p. 156.